Atmos. Meas. Tech. Discuss., 5, 8579–8607, 2012
www.atmos-meas-tech-discuss.net/5/8579/2012/
doi:10.5194/amtd-5-8579-2012

Atmospheric Measurement Techniques Discussions

Ground-based integrated path coherent differential absorption lidar measurement of CO_2: hard target return

S. Ishii[1], M. Koyama[2], P. Baron[1], H. Iwai[1], K. Mizutani[1], T. Itabe[1], A. Sato[3], and K. Asai[3]

[1]National Institute of Information and Communications Technology, 4-2-1 Nukuikitamachi, Kogenei, Tokyo 184-8795, Japan
[2]Tokyo Metropolitan University, 6-6 Asahigaoka, Hino, Tokyo 191-0065, Japa
[3]Tohoku Institute of Technology, 35-1 Yagiyamakasumi Taihaku, Sendai, Miyagi 982-8577, Japan

Received: 14 November 2012 – Accepted: 24 November 2012 – Published: 29 November 2012

Correspondence to: S. Ishii (sishii@nict.go.jp)

Published by Copernicus Publications on behalf of the European Geosciences Union.

Abstract

The National Institute of Information and Communications Technology (NICT) have made a great deal of effort to develop a coherent 2-μm differential absorption and wind lidar (Co2DiaWiL) for measuring CO_2 and wind speed. First, coherent Integrated Path Differential Absorption (IPDA) lidar experiments were conducted using the Co2DiaWiL and a hard target (surface return) located about 7.12 km south of NICT on 11, 27, and 28 December 2010. The detection sensitivity of a 2-μm IPDA lidar was examined in detail using the CO_2 concentration measured by the hard target. The precisions of CO_2 measurement for the hard target and 900, 4500 and 27 000 shot pairs were 6.5, 2.8, and 1.2 %, respectively. The results indicated that a coherent IPDA lidar with a laser operating at a high pulse repetition frequency of a few tens of KHz is necessary for measuring the CO_2 concentration of the hard target with a precision of 1–2 ppm. Statistical comparisons indicated that, although a small amount of in situ data and the fact that they were not co-located with the hard target made comparison difficult, the CO_2 volume mixing ratio measured with the Co2DiaWiL was about 5 ppm lower than that measured with the in situ sensor. The statistical results indicated that there were no differences between the hard target and atmospheric return measurements. A precision of 1.5 % was achieved from the atmospheric return, which is lower than that obtained from the hard-target returns. Although long-range DIfferential Absorption Lidar (DIAL) CO_2 measurement with the atmospheric return can result in highly precise measurement, the precision of the atmospheric return measurement was widely distributed comparing to that of the hard target return. Our results indicated that it is important to use a Q-switched laser to measure the range-gated differential absorption optical depth with the atmospheric return and that it is better to simultaneously conduct both hard target and atmospheric return measurements to enable highly accurate CO_2 measurement.

AMTD
5, 8579–8607, 2012

1 Introduction

Atmospheric carbon dioxide (CO_2) was roughly constant before the beginning of the Industrial Revolution in the mid 18th century. Population growth has resulted in an increase in the consumption of fossil fuels, and human activities led to an increase in CO_2 emission. Atmospheric CO_2 concentration has increased rapidly from 280 ppm to greater than 380 ppm since the Industrial Revolution (IPCC, 2007). Data obtained from analyses of Antarctic ice cores and atmospheric observations indicate a relationship between the increase in CO_2 concentration and atmospheric temperature (Etheriddge et al., 1996). Because of the presence of CO_2 sinks such as the oceans or terrestrial ecosystems, atmospheric CO_2 increases at only half the rate of anthropogenic CO_2 emissions; however, in nature, the spatial-scale from regional to continental and the temporal variations in the CO_2 sinks are not well understood due to limited observations (La Quéré et al., 2009). Continuous monitoring of CO_2 on a global scale is important for understanding the carbon cycle and estimating the carbon flux. Highly accurate ground-based and airborne measurements provide valuable data sets of the global CO_2 growth rate, seasonal information, hemispheric gradients, and so on. However, a lack of observation extends over a huge area. Ground-based and airborne measurements are not representative of the huge area to accurately infer carbon fluxes. Spaceborne measurement is a promising approach for globally measuring the temporal and spatial distribution of XCO_2 (column-weighted dry-air mixing ratio of CO_2). Spaceborne XCO_2 measurement with a bias-free high precision of 1–2 ppm is necessary to improve the carbon cycle. In 2009, the Greenhouse gas Observing SATellite (GOSAT) (Kuze et al., 2009), equipped with spaceborne passive sensors, was launched to continuously monitor the global total CO_2 column concentration. The Orbiting Carbon Observatory-2 (Crisp et al., 2004) and GOSAT-2 will be launched for the same purpose in the near future. However, a passive sensor is affected by the presence of aerosols and thin clouds; therefore, it tends to overestimate the optical depth of aerosols and to underestimate that of thin clouds.

AMTD
5, 8579–8607, 2012

An integrated path differential absorption (IPDA) lidar is one of the promising next-generation spaceborne sensors. The IPDA lidar uses a pulsed narrow-line width laser and a range-gated receiver. A Q-switched laser and range-gated receiver are helpful for distinguishing returns from the Earth's surface from other returns such as aerosols and clouds. A differential absorption lidar is not affected by the presence of aerosols and clouds, and it can be used in the day as well as at night at all latitudes, irrespective of season. The IPDA lidar has the potential of providing high measurement accuracy (bias close to zero), high precision (within a few ppm), ranging capability, and high sensitivity for detecting aerosol and clouds. The 1.6-μm and 2-μm spectral regions are suitable for XCO_2 measurement from space. The sensitivity of spaceborne lidar XCO_2 measurement has been investigated (Menzies and Tratt, 2003; Ehret et al., 2008; Kawa et al., 2010). The NASA Langley Research Center (LaRC) and the Japan Aerospace Exploration Agency (JAXA) developed a 1.57-μm laser absorption spectrometer (LAS) with modulated continuous wave and direct detection (Browell et al., 2010; Sakaizawa et al., 2010). NASA Goddard Space Flight Center (Abshire et al., 2010) and Deutsches Zentrum für Luft-und Raumfahrt (German Aerospace Center) (Amediek et al., 2008) used a 1.57-μm pulse laser and direct detection. Simulated weighting functions of a CO_2 absorption cross-section (Menzies and Tratt, 2003; Ehret et al., 2008) shows that, compared to the 1.57-μm spectral region, the 2.05-μm region is more sensitive to lower troposphere CO_2 distribution where the sinks and sources interact with the atmosphere. Various 2-μm lasers have been developed for spaceborne IPDA lidar CO_2 measurement (e.g. Yu et al., 2006; Sato et al., 2012). A 2.05-μm IPDA lidar is one of the most promising next-generation spaceborne sensors. The NASA Jet Propulsion Laboratory (JPL) (Spiers et al., 2011) is developing a 2.05-μm LAS with a continuous wave laser and heterodyne detection. NASA LaRC (Koch et al., 2004, 2008), the Institute Pierre Simon Laplace École Polytechnique (Gilbert et al., 2006, 2008), and the National Institute of Information and Communications Technology (NICT) (Ishii et al., 2010, 2012) reported 2.05-μm DIfferential Absorption Lidar (DIAL) by using a pulse laser, heterodyne detection, and aerosols and clouds (atmospheric return). We

AMTD
5, 8579–8607, 2012

evaluated the performance of horizontal and vertical CO_2 measurements using aerosol and cloud returns (Ishii et al., 2010, 2012). In this paper we describe the horizontal CO_2 measurement using a hard target. In the next section, we briefly describe our coherent 2-µm differential absorption and wind lidar (Co2DiaWiL) and discuss the retrieval method of CO_2 and the error analysis in Sect. 3. We explain the measurement strategy and experimental setup in Sect. 4. In Sect. 5, we describe the detection sensitivity of the IPDA lidar using experimental long-range CO_2 measurements, the statistical results of CO_2 measurements, and the comparison with the ground-based in situ measurements.

2 Coherent 2-µm differential absorption and wind lidar

The Co2DiaWiL specifications are listed in Table 1. Since the Co2DiaWiL is described in detail in our previous work (Ishii et al., 2012), we present its main characteristics. The Co2DiaWiL has a single-frequency Q-switched Tm,Ho:YLF laser with laser frequency offset locking technique, a 10-cm-aperture Mersenne off-axis telescope, a two-axis scanning device, two heterodyne detectors, and signal processing devices. The single-frequency Q-switched Tm,Ho:YLF laser with a 2.05-µm operating wavelength demonstrates 80-mJ output energy with a 150-ns pulse width (full width at half maximum (FWHM)) at a 30-Hz pulse repetition frequency. The Co2DiaWiL uses two wavelengths referred to as on- and off-line lasers for measuring CO_2 concentration. The two laser wavelengths are selected. The wavelength of the on-line laser corresponds to the center or wing of the absorption line of the target molecule, while the wavelength of the off-line laser lies in the far wing of the absorption line. We use the R30 absorption line of the $(20^\circ\ 1)_{III} \leftarrow (00^\circ\ 0)$ band of CO_2. The wavelength of the on-line laser can be set within the range of 2051.002–2051.058 nm using laser frequency offset locking. Based on the signal-to-noise ratio, we set the wavelength of the on-line laser at 2051.058 nm in order to conduct long-range CO_2 measurements. The wavelength of the off-line laser was set at 2051.250 nm. The absolute frequency stability of the injected pulsed laser is dominated by mechanical fluctuations of the piezoelectric

AMTD
5, 8579–8607, 2012

transducer (PZT) that controls resonator length. The absolute frequency stability of the injected pulsed laser is 1 MHz at most. The off-line laser is controlled only by adjusting the resonator temperature and piezoelectric movement of the output coupler element. The wavelength drift of the off-line laser is smaller than 7 pm, which corresponds to a maximum change of 0.04 % in the on-off difference absorption cross section. The interferences due to the presence of other atmospheric gases are almost negligible. The on- and off-line laser pulses are alternately switched every 1 shot. The pulsed laser beam is emitted into the atmosphere by using a 10-cm off-axis telescope and a waterproof 2-axis scanning device. The signal backscattered by moving aerosol particles or reflected by a hard target is detected using the heterodyne technique on an InGaAs-PIN photodiode. The heterodyne detection is operated under shot-noise-limited condition of about 9 dB. A small portion of the pulsed laser beam is also detected using the heterodyne technique to monitor the frequency of the outgoing laser pulse on a balanced InGaAs-PIN photodiode to monitor the frequency and lasing time of the outgoing laser. The outputs of these detectors are digitized at 500 MHz by using 8-bit analog-to-digital (AD) converters. The power spectra of the outgoing on- and off-line laser pulses and backscattered signals were obtained by 4096- and 512-point fast Fourier transform (FFT), respectively. The power spectra of on- and off-line backscattered signals were obtained using an algorithm proposed by Frehlich et al. (1997). Data related to laser pulses with a frequency difference of more than 1.25 MHz from the average intermediate frequency (i.e. 105 MHz) were discarded. The ratio of discarded laser shot pairs was only around 5 % in the emitted laser shot pairs.

AMTD
5, 8579–8607, 2012

3 Estimation of CO_2 and error analysis

The power $P_{i=\mathrm{On,Off}}(R)$ of backscattered signals from the hard target and atmosphere can be expressed as

$$P_i(R) = \frac{\xi_i \cdot P_{0,i} \cdot A \cdot \rho}{\pi \cdot R^2} \cdot \exp(-2 \cdot \int_0^R \alpha_i(r)\,\mathrm{d}r), \text{(hard target)} \quad (1)$$

$$P_i(R) = \frac{\xi_i \cdot P_{0,i} \cdot A \cdot \beta(R)}{R^2} \cdot \exp(-2 \cdot \int_0^R \alpha_i(r)\,\mathrm{d}r), \text{(atmosphere)} \quad (2)$$

where R is the range, ξ_i is the total instrument efficiency for the wavelength i, $P_{0,i}$ is the laser output power, A is the receiver area, ρ is the surface reflectance, where we assume that the surface of the hard target is Lambertian, $\alpha_i(r)$ is the extinction coefficient of the atmosphere, $\alpha_i(r)$ is defined as $\alpha_i\ (r) = \alpha_{\mathrm{atm}}(r) + \sigma_i(r)\rho_{\mathrm{CO_2}}N_{\mathrm{air}}$, where $\sigma_i(r)$ is the absorption cross section of CO_2, $\rho_{\mathrm{CO_2}}$ is the dry air volume mixing ratio of CO_2, N_{air} is the dry air number density, $\alpha_{\mathrm{atm}}(r)$ is the extinction coefficient associated with any other extinction processes, and $\beta_i(R_j)$ is the backscattering coefficient of the atmosphere. Since the on- and off-line wavelengths are sufficiently close, we can neglect the wavelength dependence of instrument efficiency, surface reflectance, and extinction coefficient except for CO_2 absorption.

The carrier-to-noise ratio CNR_i is defined as

$$\mathrm{CNR}_i = \frac{\langle P_i(R) \rangle}{\langle P_{i,N} \rangle}, \quad (3)$$

where $\langle P_{i,N} \rangle$ and $\langle P_i(R) \rangle$ are the mean power of the backscattered signal and the mean noise power. The theoretical signal-to-noise ratio $\mathrm{SNR}_i(R)$ for the squarer estimator

AMTD
5, 8579–8607, 2012

described by Rye and Hardesty (1997) is given as

$$\mathrm{SNR}_i(R) = \sqrt{N_\mathrm{L} \cdot N_\mathrm{C}} \cdot \frac{\mathrm{CNR}_i}{1 + \mathrm{CNR}_i}, \tag{4}$$

where N_C is the number of coherent cells, and N_L is the number of on- and off-line laser shots. In this paper, N_C for the atmospheric return signal is calculated using Eq. (4) described by Gilbert et al. (2006), and for the hard target it is calculated using Eq. (6.1–29) described by Goodman (2000).

By applying Eq. (1) to ranges R_1 and R_2, and to the on- and off-line wavelengths, the differential absorption optical depth (DAOD) due to CO_2 absorption in the range between R_1 and R_2 can be obtained as follows:

$$\mathrm{DAOD} = \int_{R_1}^{R_2} \rho_{\mathrm{CO}_2}(r) \cdot N_\mathrm{air}(r) \cdot \{\sigma_\mathrm{On}(r) - \sigma_\mathrm{Off}(r)\}\,\mathrm{d}r = \frac{1}{2} \cdot \log\left(\frac{P_\mathrm{On}(R_1) \cdot P_\mathrm{Off}(R_2)}{P_\mathrm{Off}(R_1) \cdot P_\mathrm{On}(R_2)}\right). \tag{5}$$

The CO_2 volume mixing ratio is obtained by assuming that ρ_CO and meteorological elements do not change between R_1 and R_2.

$$\rho_{\mathrm{CO}_2} = \frac{1}{2 \cdot N_\mathrm{air} \cdot \sigma \cdot (R_1 - R_2)} \cdot \left(\mathrm{DAOD} - \mathrm{DAOD}_{\mathrm{H}_2\mathrm{O}}\right), \tag{6}$$

$$N_\mathrm{air} = \frac{P}{k \cdot T} \cdot \frac{1}{1 + \rho_{\mathrm{H}_2\mathrm{O}}}, \tag{7}$$

where σ ($= \sigma_\mathrm{On} - \sigma_\mathrm{Off}$) is the difference between the absorption cross sections corresponding to the wavelengths of the on- and off-line lasers, P is pressure, T is temperature, k is the Boltzmann constant, $\rho_{\mathrm{H}_2\mathrm{O}}$ is the water vapor (H_2O) volume mixing ratio, and $\mathrm{DAOD}_{\mathrm{H}_2\mathrm{O}}$ is the DAOD due to the H_2O absorption between R_1 and R_2.

AMTD
5, 8579–8607, 2012

The relative error ΔDAOD/DAOD between 0 and R is given by

$$\frac{\Delta \mathrm{DAOD}(0,R)}{\mathrm{DAOD}(0,R)} \cong \frac{1}{2 \cdot \mathrm{DAOD}(0,R)} \sqrt{\frac{1}{\mathrm{SNR}_{\mathrm{On}}^2(R)} + \frac{1}{\mathrm{SNR}_{\mathrm{Off}}^2(R)}}. \quad (8)$$

The temporal cross correlation coefficient between $P_{\mathrm{On}}(R)$ and $P_{\mathrm{Off}}(R)$ is required to estimate the ΔDAOD/DAOD. Although we assume the temporal cross correlation coefficient as 0 to avoid the practical difficulties, the assumption does not affect the following discussions. The relative error ΔDAOD (R_1, R_2)/DAOD (R_1, R_2) between R_1 and R_2 can be expressed as

$$\frac{\Delta \mathrm{DAOD}(R_1,R_2)}{\mathrm{DAOD}(R_1,R_2)} \cong \frac{1}{2 \cdot \mathrm{DAOD}(R_1,R_2)} \sqrt{\frac{1}{\mathrm{SNR}_{\mathrm{On}}^2(R_1)} + \frac{1}{\mathrm{SNR}_{\mathrm{Off}}^2(R_1)} + \frac{1}{\mathrm{SNR}_{\mathrm{On}}^2(R_2)} + \frac{1}{\mathrm{SNR}_{\mathrm{Off}}^2(R_2)}}. \quad (9)$$

The relative error $\Delta\rho_{\mathrm{CO_2}}/\rho_{\mathrm{CO_2}}$ is obtained using Eq. (10), DAOD, and meteorological data as follows,

$$\frac{\Delta\rho_{\mathrm{CO_2}}}{\rho_{\mathrm{CO_2}}} = \sqrt{\left(\frac{\Delta N_{\mathrm{Air}}}{N_{\mathrm{Air}}}\right)^2 + \left(\frac{\Delta\sigma}{\sigma}\right)^2 + \left(\frac{\Delta \mathrm{DAOD}}{\mathrm{DAOD}}\right)^2}. \quad (10)$$

To compare with the results of the hard target return, the CO_2 volume mixing ratio was also calculated using atmospheric returns and the slope method (Gilbert et al., 2006) under assumptions that the CO_2 volume mixing ratio and CO_2 absorption cross sections do not change between R_1 and R_2.

4 Ground-based in situ measurements

Pressure, temperature, relative humidity, wind speed, and wind direction were measured using an automatic weather station (Vaisala WXT510) set up on the roof of a

AMTD
5, 8579–8607, 2012

four-story building at NICT (a section of the building has five stories). The average values of the meteorological data for each one-minute interval were automatically stored in a computer. The accuracies of pressure, temperature, and relative humidity wereare better than ±0.5 hPa, ±0.3 °C and ±3 %, which lead to a total error of 0.1 % in the CO_2 volume mixing ratio on the DIAL measurement. Additional measurements of CO_2 and H_2O concentrations were carried out at one-minute intervals with an in situ sensor (LI-COR Model LI-840, non-dispersive infrared CO_2/H_2O gas analyzer). The in situ sensor was installed in an observation room on the fifth-floor roof of the same building at NICT. Air entered the sensor at a flow rate of 1 L min^{-1} through an inlet located approximately 2 m above the roof. The inlet for the in situ sensor was about 4 m higher than the automatic weather station. Calibrations were made before measurements with 0, 358, and 452 ppm CO_2 standard reference gases. The accuracy of the analyzer was better than 1.5 %, and the root-mean-square value of the measured fluctuation was less than 1 ppm for a CO_2 volume mixing ratio of 370 ppm and for one-second filtering. In situ measurement was recorded after one-minute integration. The measured CO_2 data were compared with the results obtained from DIAL measurement.

5 Experimental hard target measurement

Figure 1a and b show the detailed topography and cross section around the target area. The laser beam was directed horizontally southward by using the 2-axis scanning device from NICT. It propagated 20 to 40 m above the surface and went through a commercial area, highway, and the Tama river before it hit the hard target surface. The hard target is located approximately 7 km south of NICT. Figure 2a shows an example of the outgoing off-line laser pulse signal (gray line) and the off-line return signal (black line) obtained using 500-MHz-sampling-rate 8-bit AD converters. Arrows a and b indicate the peak time of lasing with Q-switching and the signal from the hard target. Figure 2b and c show the square of the intermediate-frequency (IF) signals of the outgoing off-line laser pulse and the off-line return signal. We define the range between the

AMTD
5, 8579–8607, 2012

Co2DiaWiL and the hard target as the time difference at the two peaks. Figure 3a and b show examples of the range between the Co2DiaWiL and the hard target measured using the on- and off-line lasers from 01:50 to 01:55 JST on 11 December 2010. The range fluctuations shown in Figs. 3a through c were induced mainly by speckle-induced intensity fluctuation. We also believe that unstable pointing (e.g. swaying branches) of the laser beam at the hard target might have caused range fluctuations. The average ranges for the on- and off-line lasers for 1-min intervals were 7.089 (± 0.010)–7.091 (± 0.011) and 7.091 (± 0.012)–7.093 (± 0.012) km, and the average ranges for 5-min interval were 7.090 (± 0.011) and 7.092 (± 0.012) km. The pulse width of 150 nsec corresponds to the range resolution of 0.023 km. Uncertainties of ±0.012 km were expected. The frequency distributions of the measured range for the on- and off-line lasers were constructed for the on- and off-line lasers and are shown in Fig. 3c. This figure also shows that the measured range was distributed widely between 7.08 km and 7.11 km. We used the range resolution of 150 m to avoid speckle-induced intensity fluctuation for determining a correct range. The hard target was included at a range of 7.12 (± 0.075) km.

Figure 4 shows the CNR_i's for the on-line (gray line) and off-line (black line) laser pulses obtained from the hard target and atmospheric returns. The CNR_i was calculated using the power spectra of the backscattered signals. The CNR_i's of the on- and off-line laser decreased slowly with increasing range up to 6.97 km, and a CNR_i higher than 30 dB was observed at a range of 7.12 km. There are large differences more than 30 dB in the CNR at the ranges of 6.97 and 7.12 km. The hard target return was much stronger than the atmospheric return. Although the power of the atmospheric return could be included at the range of 7.12 km, the power was determined by the power of the hard target return signal.

The relation between the range and DAOD (R_1 = 0.974 km) for various shot pairs are shown in Fig. 5a. The DAOD for the 900 and 4500 shot pairs increased linearly with the range up to roughly 5 km, but for the 27 000 shot pairs, it increased linearly with the range up to about 7 km. The DAOD for the 900 and 4500 shot pairs showed large

AMTD
5, 8579–8607, 2012

fluctuations for distances greater than 4 km due to the decrease in the CNR_i, while for the 27 000 shot pairs, no large fluctuations were found. Figure 5b shows the relation between the range and relative error of the DAOD for the three shot pairs. The minimum relative errors of the DAOD for the three laser shot pairs in the range of 1 to 7 km were 13, 5.8, and 2.7 %, respectively. The relative error at short ranges was large due to the small DAOD and low heterodyne efficiency. The heterodyne detection measurement was also limited by speckle-induced noise. The relative error of the DAOD at the range of 7.12 km was about two times lower than the minimum relative errors due to the high CNR_i. The relative errors of the DAOD for the three laser shot pairs at the hard target bin were 6.5, 2.8, and 1.2 %, respectively.

The probability density functions (PDFs) of on- and off-line backscattered power follows a gamma density function and N_C is equal to the normalized variance of the backscattered power, which is calculated using Eq. (6.1–29) described by Goodman (2000). The PDFs for on- and off-line normalized power for the 27 000 shot pair measured from 01:50 to 02:20 JST on 11 December 2010 are shown in Fig. 6. The PDF follows a gamma density function with $N_C = 1.9$ calculated using Eq. (6.1–29). The calculated N_C for the atmospheric return amounts to 6.7 using a pulse width of 150 ns and a range gate duration of 1000 ns. The calculated N_C for the atmospheric return is 3.5 times larger than the N_C for the hard target return. Therefore, the N_C for the hard target return is limited to improving the signal-to-noise ratio. Figure 7 shows the relation between the average number of pulses and relative error of the DAOD for various shot pairs. We compared the theoretical and experimental values of the relative error of the DAOD. The theoretical values were calculated using Eqs. (4) and (9), and the results are shown as a black solid line in Fig. 7. The relative error of the DAOD by signal segmental averaging was found to decrease as $N_L^{-1/2}$. To obtain a relative error of 1–2 ppm under the assumptions that relative errors of N_{air} and σ were 0 %, our results indicate that the coherent IPDA lidar with the laser at a pulse repetition frequency of a few tens of KHz may be necessary to develop a coherent IPDA lidar.

AMTD
5, 8579–8607, 2012

The horizontal experimental CO_2 measurements were done continuously from 12:10 JST on 27 December to 16:02 JST on 28 December 2010. The temporal variations of the CO_2 volume mixing ratio measured using the Co2DiaWiL and the in situ sensor are shown in Figs. 8a and b. The crosses and open circles show results obtained from hard target and atmospheric returns, respectively. The gray line shows the data obtained from the in situ sensor. The time-series of N_C's for on- and off-line backscattered power is shown in Fig. 8c. The data show that the N_C's for on- and off-line backscattered power were 1.5–1.9 during the day and 1.7-2.2 during at night. The N_C's were roughly constant during the experimental period. The 4500 shot pairs were used to estimate the CO_2 volume mixing ratios for both hard target and atmospheric returns. The CO_2 volume mixing ratio for the hard target return was obtained with a DAOD between 0.974 and 7.12 km and Eq. (5). The CO_2 volume mixing ratio for the atmospheric return was estimated for a column range from 0.974 to 6.97 km by using the slope method. There are 40 range-gated bins in the column range. The precision values of the Co2DiaWiL measurements for the hard target and atmospheric returns shown in Figs. 8a and b were in the range of 2.8–5.3 and 1.5–11.0 %. Although meteorological data were not obtained close to the target surface, the data measured using our automatic weather station were used to calculate the absorption cross section of CO_2 for the on- and off-line lasers. Since the difference between the pressure measured using our automatic weather station and that at the hard target was smaller than 1 hPa, the pressure induced error on the retrieved CO_2 volume mixing ratio was negligible. However, if the temperature difference between the two points were larger than 1 K, it would result in a difference larger than 0.5 % in the CO_2 volume mixing ratio. The error due to the difference between on- and off-line absorption cross sections was 0.07 % in the CO_2 volume mixing ratio on the Co2DiaWiL measurement. The frequencies of differences between the Co2DiaWiL measurements for the hard target and atmospheric returns and the 5-min running averages of the in situ sensor are shown in Fig. 9. The CO_2 volume mixing ratio estimated from the hard target and atmospheric returns shows that the Co2DiaWiL CO_2 measurements are not

AMTD
5, 8579–8607, 2012

always lower/higher than the in situ sensor measurements. The average differences between the Co2DiaWiL measurements for the hard target and atmospheric returns were −4.6 and −5.0 ppm lower than the 5-min running averages of the in situ sensor. The difference of 5 ppm might be interpreted as a bias. The root-mean-square of the absolute values of difference between the Co2DiaWiL measurements for the hard target and atmospheric returns and the 5-min running averages of the in situ sensor were 26.1 and 25.9 ppm. These statistical results indicate that the root-mean-square of the absolute values of the difference of the hard target return measurement was almost as the same as those of the atmospheric return measurement. The causes of the differences between the Co2DiaWiL and the in situ sensor are sampling volume, sampling location, and sampling height. It should also be emphasized that these results were just an isolated comparison. Figure 10 shows the precision frequencies of the Co2DiaWiL measurements for the hard target and atmospheric returns conducted on 27 and 28 December. The precisions of the hard tarraget return measurement were mostly less than 3.8 %. On the other hand, the high precision frequencies of the atmospheric return measurement were less than approximately 3.3 %. It should be noted that, although the long-range DIAL CO_2 measurement with the atmospheric return can result in highly precise measurement, precision depends strongly on the fluctuation of the DAOD due to the decrease in the CNR. An important point is that the long-range DIAL CO_2 measurement with the hard target return measurement would be better for maintaining data quality.

6 Conclusions

We used the Co2DiaWiL with a 2-μm single-frequency Q-switched laser with laser frequency offset locking to examine the detection sensitivity of a 2-μm IPDA lidar. Experimental horizontal CO_2 measurements were conducted using hard target (surface) and atmospheric (aerosol) returns in the western part of Tokyo on 11, 27 and 28 December 2010. The CO_2 concentration was first measured with the 2-μm coherent IPDA

AMTD
5, 8579–8607, 2012

lidar. The hard target is located about 7.12 km south of NICT. The results obtained from the hard target return were examined in detail and compared with those measured from the atmospheric return and the in situ sensor. The range measured using the Co2DiaWiL showed a large fluctuation related mainly to speckle-induced intensity fluctuation. For coherent lidar, it is difficult to measure the range with a high precision of less than 1 m due to the long laser pulse width. The precision of the range measured using the Co2DiaWiL was within 0.012 km, which corresponded to the laser pulse width of 150 nsec. The precisions of CO_2 measurement due to the DAOD for the hard target and 900, 4500 and 27 000 shot pairs were 6.5, 2.8, and 1.2 %. The results indicated a laser operating at a high pulse repetition frequency of a few tens of KHz may be necessary for the coherent IPDA lidar. Threfore, significant laser and optical device improvements are necessary for future CO_2 measurements with the coherent IPDA lidar. Although the averages values of the differences between the Co2DiaWiL measurements were about 5 ppm lower than the 5-min running averages of the in situ sensor, the comparison between the Co2DiaWiL and in situ sensor CO_2 measurements was difficult from the point of the view of the one isolated comparison. Statistical comparisons indicated that there are no large differences between hard target and atmospheric return measurements. The precision of the hard target return measurement was slightly worse than that of the atmospheric return measurement. The N_C for the hard target return was limited to the improvement of the signal-to-noise ratio. The results indicate that long-range DIAL CO_2 measurement with atmospheric return can enable highly precise measurement. The precision of long-range DIAL CO_2 measurement with atmospheric return depends strongly on the fluctuation of the DAOD. The long-range DIAL CO_2 measurement with hard target return may exhibit better data quality than that with atmospheric return. The results presented in this paper indicate that it is important to use a Q-switched laser to conduct range-resolved DAOD measurement with atmospheric return and that it is better to simultaneously conduct both hard target and atmospheric return measurements to enable CO_2 measurement with bias-free high precision. The

AMTD
5, 8579–8607, 2012

IPDA lidar with a Q-switched laser and a range-gated receiver has a great advantage in terms of discussing uncertainty due to the presence of aerosols and clouds.

References

Abshire, J. B., Riris, H., Allan, G. R., Weaver, C. J., Mao, J., Sun, X., Hasselbracj, W. E., Kawa, S. R., and Biraud, S.: Pulsed airborne lidar measurements of atmospheric CO_2 column absorption, Tellus, 62B, 770–783, 2010.

Amediek, A., Fix, A., Wirth, M., and Hert, G.: Development of an OPO system at 1.57 µm for integrated path DIAL measurement of atmospheric carbon dioxide, Appl. Phys., B92, 295–302, 2008.

Browell, E. V., Dobler, J., Kooi, S. A., Choi, Y., Harrison, F. W., Moore III, B., and Zaccheo, T. S.: Airborne validation of laser remote measurements of atmospheric carbon dioxide, Proc. 25th Int. Laser Radar Conf., 1, S6O–03, 2010.

Crisp, D., Atlas, R. M., Breon, F.-M., Brown, L. R., Burrows, J. P., Ciais, P., Connor, B. J., Doney, S. C., Fung, I. Y., Jacob, D. J., Miller, C. E., O'Brien, D., Pawson, S., Randerson, J. T., Rayner, P., Salawitch, R. J., Sander, S. P., Sen, B., Stephens, G. L., Tans, P. P., Toon, G. C., Wennberg, P. O., Wofsy, S. C., Yung, Y. L., Kuang, Z., Chudasama, B., Sprague, G., Weiss, B., Pollock, R., Kenyon, D., and Schroll, S.: The Orbiting Carbon Observatory mission, Adv. Space. Res., 34, 700–709, 2004.

Ehret, G., Kiemle, C., Wirth, M., Amediek, A., Fix, A., and Houweling, S.: Space-borne remote sensing of CO_2, CH_4, and N_2O by integrated path differential absorption lidar: A sensitivity analysis, Appl. Phys., B90, 593–608, 2008.

Etheridge, D. M., Steele, L. P., Langenfelds, R. L., Francey, R. J., Barnola, J.-M., and Morgan, V. I.: Natural and anthropogenic changes in atmospheric CO_2 over the last 1000 years from air in Antarctic ice and firn, J. Geophys. Res., 101, 4115–4128, 1996.

Intergovernmental Panel on Climate Change (IPCC), Climate change 2007: The Physical Science Basis: Contribution of Working Group I to the Fourth Assessment Report of the Intergovernmental Panel on Climate Change, edited by: Solomon, S., Qin, D., Manning, M., Chen, Z., Marquis, M., Averyt, K. B., Tignor, M., and Miller, H. L., Cambridge University Press, Cambridge, UK and New York, NY, USA, 996 pp., 2007.

AMTD
5, 8579–8607, 2012

Gilbert, F., Flamant, P. H., Bruneau, D., and Loth, C.: Two-micrometer heterodyne differential absorption lidar measurements of the atmospheric CO_2 mixing ratio in the boundary layer, Appl. Opt., 45, 4448–4458, 2006.

Gilbert, F., Flamant, P. H., Cuesta, J., and Bruneau, D.: Vertical 2-µm heterodyne differential absorption lidar measurements of mean CO_2 mixing ratio in the troposphere. J. Atmos. Ocean. Technol., 25, 1477–1499, 2008.

Goodman, J. W.: Statistical Optics, Wiley Classics Library, New York, 2000.

Ishii, S., Mizutani, K., Fukuoka, H., Ishikawa, T., Baron, P., Iwai, H., Aoki, T., Itabe, T., Sato, A., and Asai, K.: Coherent 2-µm differential absorption and wind lidar with conductively-cooled lLaser and two-axis scanning device, Appl. Opt., 49, 1809–1817, 2010.

Ishii, S., Mizutani, K., Baron, P., Iwai, H., Oda, R., Itabe, T., Fukuoka, H., Ishikawa, T., Koyama, M., Tanaka, T., Morino, I., Uchino, O., Sato, A., and Asai, K.: Partial CO_2 Column-averaged Dry-air Mixing Ratio from Measurements by coherent 2-µm differential absorption and wind lidar with Laser Frequency Offset Locking, J. Atmos. Ocea. Technol., 29, 1169–1181, doi.org/10.1175/JTECH-D-11-00180.1, 2012

Kawa, S. R., Mao, J., Abshire, J. B., Collatz, G. J., Sun, X., and Weaver, C. J.: Simulation studies for a space-based CO_2 lidar mission, Tellus, 62B, 759–769, 2010.

Koch, G. J., Barnes, B. W., Petros, M., Beyon, J. Y., Amzajerdian, F., Yu, J., Davis, R. E., Ismail, S., Vay, S., Kavaya, M. J., and Singh, U. N.: Coherent differential absorption lidar measurements of CO_2, Appl. Opt., 43, 5092–5099, 2004.

Koch, G., Beyon, J. Y., Gilbert, F., Barnes, B. W., Ismail, S., Petros, M., Petzar, P. J., Yu, F. J., Modlin, E. A., Davis, K. J., and Singh, U. N.: Side-line tunable laser transmitter for differential absorption lidar measurements of CO_2: Design and application to atmospheric measurements, Appl. Opt., 47, 944–956, 2008.

Kuze, A., Suto, H., Nakajima, M., and Hamazaki, T.: Thermal and near infrared sensor for carbon observation Fourier-transform spectrometer on the Greenhouse Gases Observing Satellite for greenhouse gases monitoring, Appl. Opt., 48, 6716–6733, 2009.

Le Quéré, C., Raupach, M. R., Canadell, J. G., Marland, G., Marland, G., Bopp, L., Ciais, P., Conway, T. J., Doney, S. C., Feely, R. A., Foster, P., Friedlingstein, P., Gurney, K., Houghton, R. A., House, J. I., Huntingford, C., Levy, P. E., Lomas, M. R., Majkut, J., Metzl, N., Ometto, J. P., Peters, G. P., Prentice, I. C., Randerson, J. T., Running, S. W., Sarmiento, J. L., Schuster, U., Sitch, S., Takahashi, T., Viovy, N., van der Werf, G. R., and Woodward, F. I.: Trends in the sources and sinks of carbon dioxide, Nat. Geosci., 2, 831–836, doi:10.1038/ngeo689, 2009.

AMTD
5, 8579–8607, 2012

Menzies, R. T. and Tratt, D. M.: Differential laser absorption spectrometry for global profiling of tropospheric carbon dioxide: selection of optimum sounding frequencies for high-precision measurements, Appl. Opt., 42, 6569–6577, 2003.

Sakaizawa, D., Kawakami, S., Nakajima, M., Sawa, Y., and Matsueda, H.: Ground-based demonstration of CO_2 remote sensor using 1.57 μm differential laser absorption spectrometer with direct detection, J. Appl. Remote. Sens., 4, 043548, doi:10.1117/1.3507092, 2010.

Sato, A., Miyake, Y., Asai, K., Ishii, S., and Mizutani, K.: Tunable, Q-switched Tm,Ho:LLF laser with a conductively cooled triangular prism rod, Appl. Opt., 51, 1236–1240, 2012.

Spiers, G. D., Menzies, R. T., Jacob, J., Christensen, L. E., Phillips, M. W., Choi, Y., and Browell, E. V.: Atmospheric CO_2 measurements with a 2 μm airborne laser absorption spectrometer employing coherent detection, Appl. Opt., 50, 2098–2111, 2011.

Yu, J., Trieu, B. C., Petros, M., Bai, Y., Petzar, P. J., Koch, G. J., Singh, U. N., and Kavaya, M. J.: Advanced 2-μ m solid-state laser for wind and CO_2 lidar applications, Society of Photo-Optical Instrumentation Engineers (SPIE) Conference Series, edited by: Singh, U. N., vol. 5575 of Society of Photo-Optical Instrumentation Engineers (SPIE) Conference Series, 6409, C4091–C4091, doi:10.1117/12.696908, 2006.

AMTD
5, 8579–8607, 2012

Table 1. Specifications of coherent 2-μm differential absorption and Doppler wind lidar.

Transmitter	
Laser	Tm,Ho;YLF
Wavelength	2051.058 nm (On)/2051.250 nm (Off)
Pulse energy	50-80 mJ/pulse (Operational)
Pulse width (FWHM)	150 ns
Pulse repetition	30 Hz
Polarization	Circular
Receiver	
Telescope type	Mersenne off-axis
Diameter	0.1 m
Magnification	10
Detector for reference signal	Balanced InGaAs-PIN photodiode
Detector for backscattered signal	InGaAs-PIN photodiode
Scanner	
Scanning range	Azimuth −10° to 370° Elevation −20° to 200°
Effective clear aperture	0.1 m
Scanning resolution	0.01°
Scanning speed	up to 60° s^{-1}
Signal processing	
Signal sampling frequency	500 MHz
Resolution	8 bits
FFT-point (reference)	4096
FFT-point (signal)	512
Range resolution	150 m

AMTD
5, 8579–8607, 2012

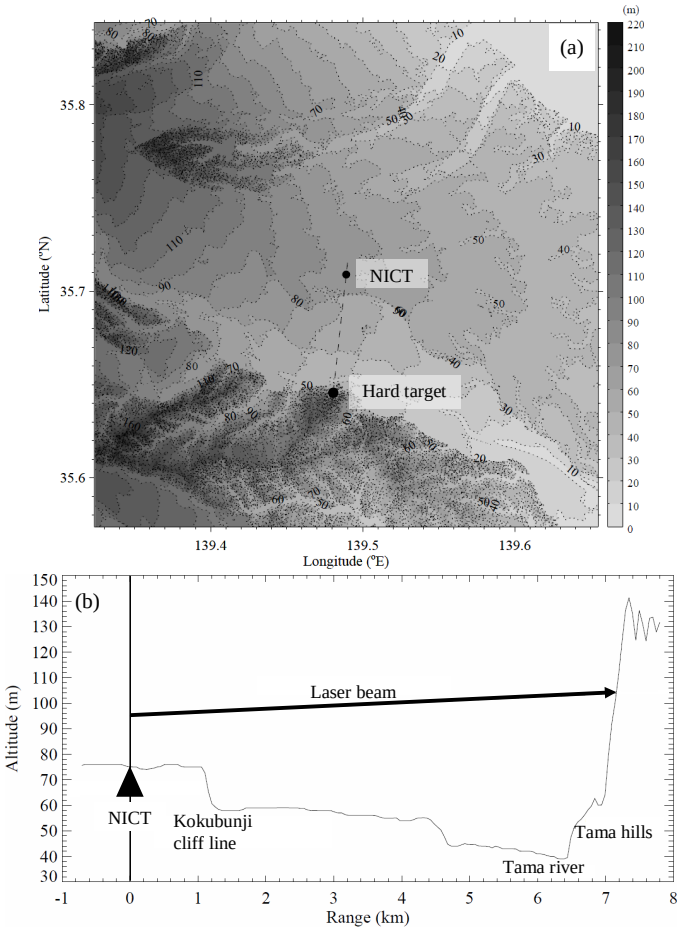

Fig. 1. (a) Map of area around NICT, hard target, and investigated areas. Contour lines are represented at intervals of 10 m. **(b)** Cross section of topography data from NICT towards hard target.

AMTD
5, 8579–8607, 2012

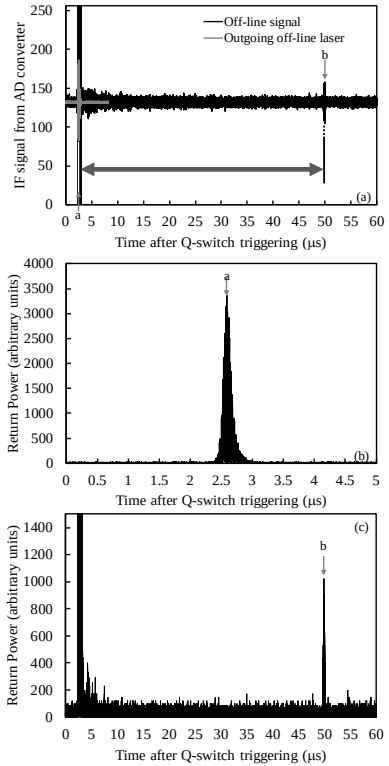

Fig. 2. (a) Outgoing laser pulse and atmospheric return signals versus time recorded using 8-bit AD converters. **(b)** A-scope display of outgoing laser pulse. **(c)** A-scope display of atmospheric and hard target return signals. Labels “a” and “b” show peak location for outgoing laser pulse and hard target return signal.

AMTD
5, 8579–8607, 2012

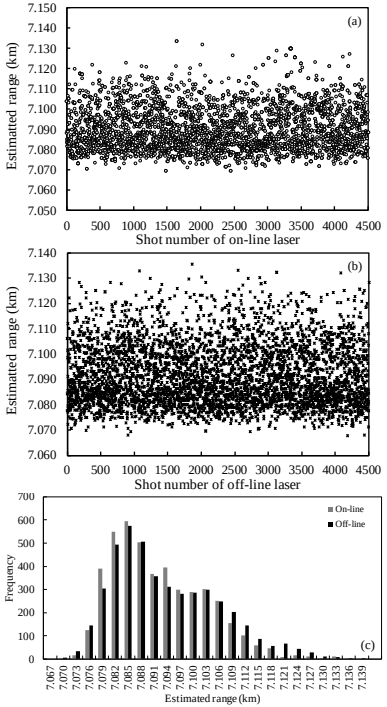

Fig. 3. Range estimated from time difference between labels “a” and “b” in Fig. 2a for **(a)** on-line laser pulse and **(b)** off-line laser pulse and **(c)** frequency of estimated range for on- and off line laser pulse. Measurements were conducted from 01:50 to 01:55 JST on 11 December 2010.

AMTD
5, 8579–8607, 2012

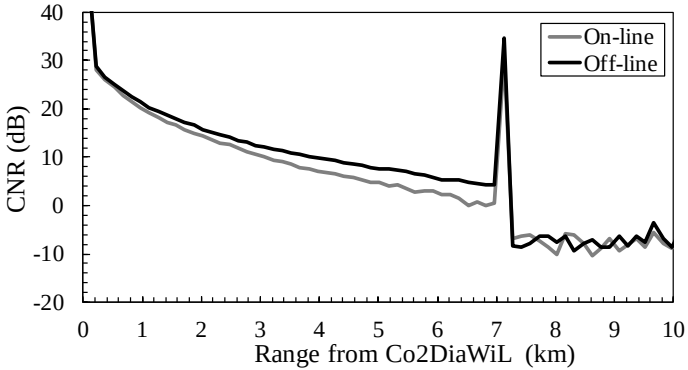

Fig. 4. Carrier-to-noise ratio (CNR_i) for on- and off-line laser pulses. Measurements are same as those in Fig. 3. Peaks at 7.1 km shows CNR of hard target return.

AMTD
5, 8579–8607, 2012

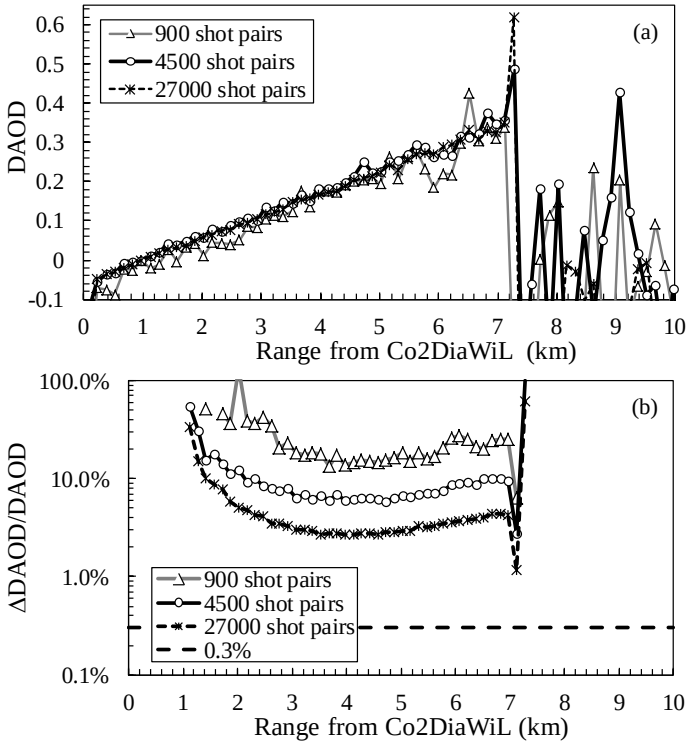

Fig. 5. Relation between range and **(a)** differential absorption optical depth (DAOD) and **(b)** relative error of DAOD for 900 (open triangle), 4500 (open circle), and 27 000 (asterisk) shot pairs. Measurements were conducted from 01:50 to 02:20 JST on 11 December 2010. Dashed line shows relative error of DAOD of 0.3 % corresponding to 1 ppm in CO_2 volume mixing ratio.

AMTD
5, 8579–8607, 2012

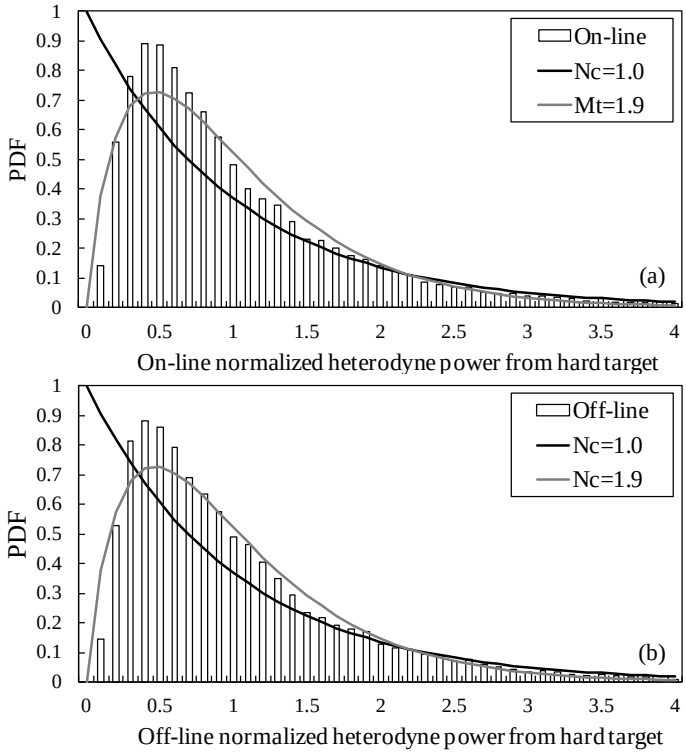

Fig. 6. Histgram of PDFs for **(a)** on-line and **(b)** off-line normalized heterodyne power for 27 000 returns from 7.12-km-distant hard target. Measurements are same as those in Fig. 5. PDF follows a gamma function with N_c = 1.9, plotted as gray solid line. Solid line is a negative exponential distribution.

AMTD
5, 8579–8607, 2012

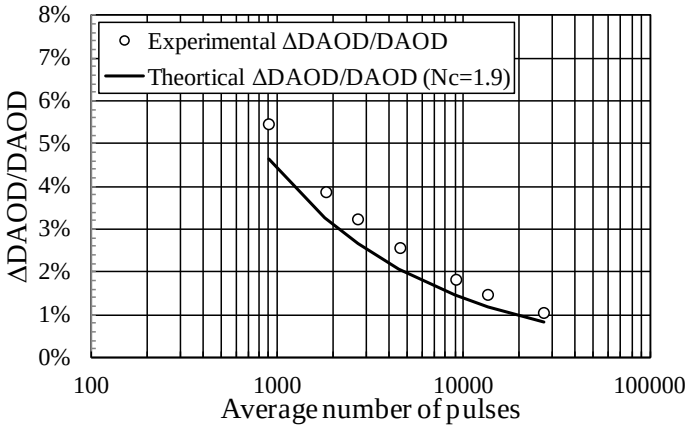

Fig. 7. Calculated relative error of DAOD for various shot pairs. Measurements are same as those in Fig. 5.

AMTD
5, 8579–8607, 2012




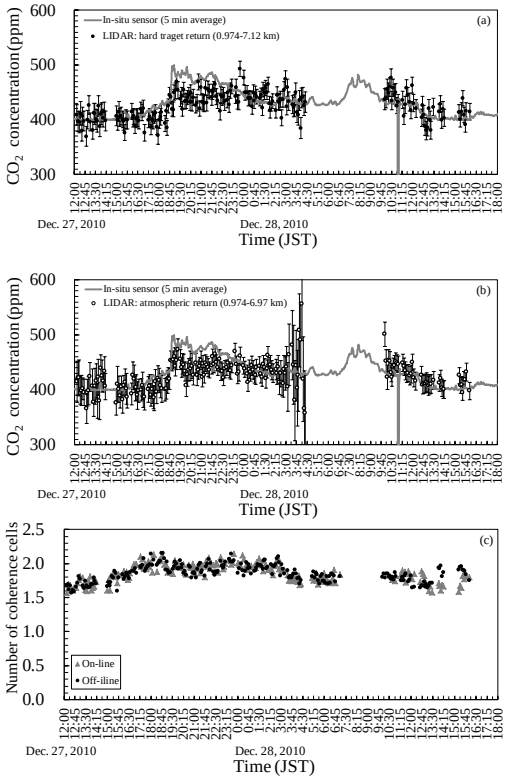

Fig. 8. Temporal variations of CO_2 concentrations measured using Co2DiaWiL and in situ sensor on 27 and 28 December 2010: **(a)** hard target return and **(b)** atmospheric return. Laser frequency offset was 6.5 GHz for horizontal CO_2 measurement. **(c)** Time-series of N_c: (•) on- and (▲) off-line laser pulse.

AMTD
5, 8579–8607, 2012

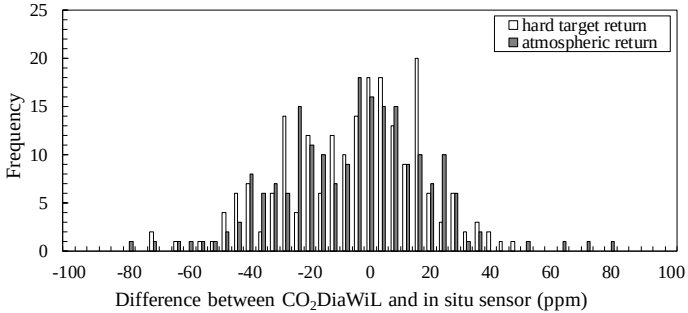

Fig. 9. Frequency of differences between Co2DiaWiL measurements and 5-min running averages of in situ sensor.

AMTD
5, 8579–8607, 2012

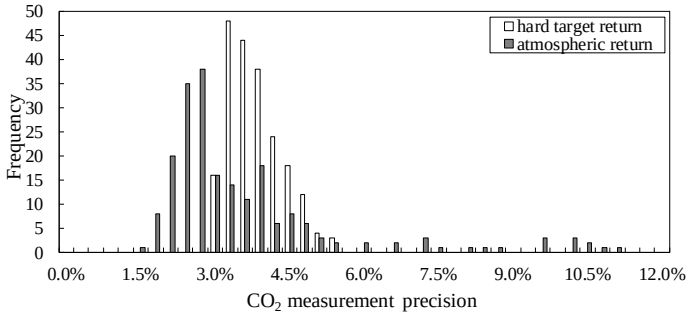

Fig. 10. Frequency of Co2DiaWiL measurement precision for hard target and atmospheric return.

AMTD
5, 8579–8607, 2012